Leadership in Sustainable Infrastructure
Leadership en Infrastructures Durables

Vancouver, Canada
May 31 – June 3, 2017/ *Mai 31 – Juin 3, 2017*

DETECTION AND CHARACTERIZATION OF SURFACE CRACKS AND DEFECTS IN CONCRETE STRUCTURES USING VARIOUS NDTS

Azarsa, Pejman[1], Gupta, Rishi[2,4], Biparva, Alireza[3]
[1] PhD candidate at University of Victoria, Victoria, B.C. Canada
[2] Assistant Professor at University of Victoria, Victoria, B.C. Canada
[3] Research and Development Manager, Kryton International Inc, Vancouver, B.C. Canada
[4] guptar@uvic.ca

ABSTRACT: Concrete is the most versatile and durable construction material; however, due to many factors such as steel corrosion and service loading anomalies in concrete are inevitable. Developing defects within the concrete matrix creates pathways for aggressive agents to initiate deterioration processes and endanger the structure service life. Thus, over the past few years, many techniques have been developed to evaluate the state of various civil engineering structures for detecting internal voids, surface defects or cracks in a non-destructive way. Among these techniques, Infrared Thermography (IRT) is available to engineers for Non-Destructive Testing (NDT) of concrete elements. Voids and irregularities in concrete affect heat flow through the material and these changes in heat flow cause localized differences in surface temperature. IRT has certain limitations concerned with problems of the emitted radiation from the surface, but at the same time the method was proven useful when used in conjunction with NDT methods that enable defect detection. The main goal of this work is to detect the surface temperature distribution captured by the IR camera in conjunction with Electrical Resistivity (ER) readings to determine and quantify the position of the defect/voids. For experimental investigations, a range of artificial defects has been induced into steel reinforced concrete slabs (1.8 × 0.46 m) at 0.1 m and 0.15 m in thickness. The results are combined maps of internal defects/surface voids using both techniques allowing for a comprehensive assessment for concrete service repairs.

1 INTRODUCTION

Defects in concrete structures can be product of reinforcement corrosion, or structural loading. These defects may not be visually detected by naked eyes until they break surface and allow rapid structure's deterioration by creating a pathway for aggressive agents to infiltrate. Detection of this type of damage is essentially demanded for early assessment of material's condition. In order to investigate various types of defects, a particular Non-destructive testing (NDT) technique (e.g. infrared thermography) can be employed according to the physical properties of the material to achieve the most reliable results. However, combining a number of NDT methods is considered as one of the most suitable ways to ameliorate the quality of civil structures' diagnosis. An example of this case is described in (Büyüköztürk 1998), where infrared thermography has been used together with acoustic imaging, radiography tomography and Ground Penetrating Radar (GPR) to investigate the location and depth of various anomalies in concrete structures (Büyüköztürk 1998). Also, in Washer work (Washer 1998), in order to detect cracks in the USA highway bridges, both Infrared Thermography (IRT) technique and radar were employed. It is stated that infrared is a valuable tool to test areas, which the radar cannot reach. In the USA, the suitable strategy for conducting

an infrared survey has been published in ASTM D4788 standard (ASTM D4788-03 2013). Although, various works have been undertaken to quantify infrared images, but in the present case, cracking/defect detection is attempted by the combination of IRT, used as a global monitoring tool to indicate the possible areas of subsurface defects and Electrical Resistivity (ER) measurements which are influenced mainly by the connectivity of concrete pore structures especially in the cracks' region.

Infrared Thermography (IRT) technique is based on the measurement of the radiant thermal energy distribution which is emitted from a target. Non-homogeneities in the near surface region of a structural element will result in many cases in measurable temperature differences. The thermal energy which is measured by the thermal sensor of an IR camera consists of the energy emitted by the target itself as well as the energy reflected by the surroundings via the object's surface. As an advanced device, an IR camera is calibrated to measure the emissive power of surfaces in a region with various temperature ranges and builds a series of the thermal distribution images (Balaras and Argiriou 2002). The emitted radiation from the region of interest is focused by the optics onto the IR sensor and the electrical response signal is converted into a digital image. The different thermal anomalies specified by the different colors in the image, such as increase and decrease of surface temperatures or retained heat arise when a crack, moisture accumulation, or any other defected area is presented. In civil engineering, the application of IRT is an established non-destructive method for the detection of moisture in the near surface region (Poblete and Acebes Pascual 2007), the detection of plaster delamination (Meola and Carlomagno 2006), and the localization of voids and other irregularities in the near surface region (Maierhofer, Arndt, and Röllig 2007), and many more. Therefore, it fulfils the first prerequisite of testing because it can monitor a large surface area by just one thermographic image. When the defect is identified, another technique can be used for more accurate characterization of its depth. ER can be the most promising technique for this task, since presence of cracks changes the pore connectivity, and thus its electrical conductivity (Ranade et al. 2014).

Electrical Resistivity (ER) measurement techniques are also becoming more popular especially for field evaluations due to its simplicity, rapidness, and cost during test conduction (Azarsa and Gupta, 2017). ER is a material property that can be employed for several purposes, one of which is to identify early age characteristics of fresh concrete. It is also a suitable tool for condition surveying and assessment of concrete properties. Since electrical current is carried by dissolved charged ions flowing into the concrete pore solution, it is a decent indicator of concrete pore structures (Sengul 2014). Additionally, ER method can be considered as an index to determine the moisture content and the connectivity of the micro-pores in the concrete (Rajabipour, Weiss, and Abraham 2004). One of the important factors affecting the measurements is environmental conditions such as temperature, rainfall and relative humidity. Also, the moisture content of concrete highly influences the electrical resistivity readings. Hence, once the moisture content reduces in concrete, the resistivity increases significantly. Moreover, it is a reliable test method to detect and monitor the initiation and propagation of cracks in concrete since they change the connectivity of concrete pore structure, and thus its electrical conductivity (Ranade et al. 2014). Therefore, detecting cracks/defects when all these influencing parameters should be considered for on-site resistivity measurements and infrared examination, is not a simple task.

In this study, the findings of an investigation of determining correlation between IRT and ER techniques will be presented. The background and fundamentals of both NDT methods, for the beginners and non-experts for easy understanding of the subject, are thoroughly explained.

2 BACKGROUND AND THEORY

2.1 Basic concepts of thermography NDT

As an object is exposed to a heat source, its temperature is started to increase due to energy absorption. Through a dynamic process which includes conduction, convection, and radiation, the heat between the object and the surrounding environment typically exchanges. Hence, heat radiation may be observed through the propagation of electromagnetic waves composing a range of wavelengths (Cheng, Cheng, and Chiang 2008). In the electromagnetic spectrum, shown in Figure 1, infrared radiation is located between visible and microwaves which its wavelength ranges from 0.75 to 14 μm. From the NDT viewpoint, the

principle behind IRT technique in any material is to monitor the variations in its thermal properties, especially those caused by a subsurface defect (Cheng, Cheng, and Chiang 2008). An infrared camera can detect the infrared radiation from an object surface. Thus, changes on the surface temperature, which may also be affected by the subsurface defects, can be localized using the thermal images. IRT technique can be divided into two approaches: passive thermography and active thermography. Further details of these approaches has been discussed in the following sections.

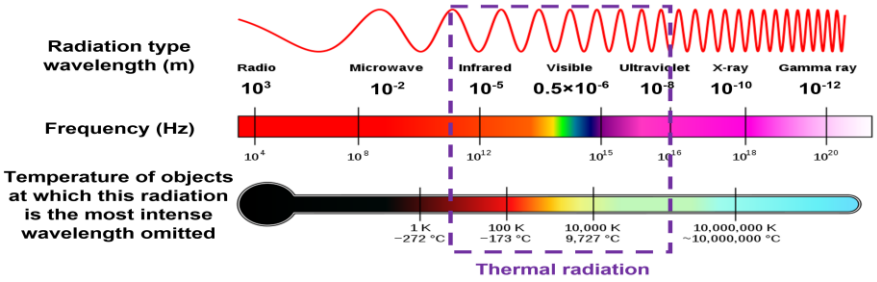

Figure 1: Electromagnetic spectrum

2.1.1 **Passive thermography**

Thermal variations of a material can be determined in this approach by means of an infrared vision device without any external thermal sources. In this case, the regions of interest are inherently at a higher or lower temperature than the background. Passive thermography is considered rather as a qualification test because the detection of the thermal anomalies' locations is the basic objective of this method. Due its non-contact nature, passive thermography is a suitable technique for evaluation of the building envelope in historical structures while the state of corrosion in real time can be simply defined. Entrapped moisture can also be easily detected using IRT technique as those regions show cooler temperature in the thermal image. Generally, in porous materials like concrete, presence of moisture increases thermal conductivity of such materials and decreases thermal resistance, thus producing a sort of thermal bridge (Titman 2001).

2.1.2 **Active thermography**

In contrast to passive thermography, in active thermography approach, the temperature difference is determined by exposing the structure to an external stimulus which forms any type of external heat source like lamps, hot packs, and ovens (Kylili et al. 2014). Active thermography technique is differentiated by nature of stimulus into Pulsed Thermography (PT) and Lock-in Thermography (LT).

2.1.2.1 Pulsed Thermography (PT)

PT is an efficient non-destructive technique of testing structure materials. This method measures by thermal stimulation while applying a heating pulse and monitoring the temperature variation with IR camera on the material's surface during heating and cooling transient phases (Maldague 2001; Carosena Meola and Giovanni M Carlomagno 2004; Sun 2006). PT is the most popular technique in diagnosing non-homogeneities in structures, and numerous studies have been conducted regarding the assessment of the structures condition. Non-homogeneities such as voids and delamination are characterised by various thermal properties. When present in material matrix, non-homogeneities effect the surface temperature map and thus resulting their detection. As an example, Brown and Hamilton (Brown and Hamilton 2013) preformed their IR examinations by heating the concrete specimens with halogen lamps. The core objective of their work was to detect the interruption of the transient heat flow when a defect area is encountered. In order to be able to accurately interpret the anomaly in size, position and physical properties, a quantitative interpretation of the thermal data is required (Sun 2006). In civil engineering field, this method is generally employed where the target's quantitative characterization is feasible.

2.1.2.2 Lock-in Thermography (LT)

LT can be carried in two different formats: stimulation with a heating lamp categorised as optical lock-in thermography (OLT) or stimulation with elastic waves called ultrasound lock-in thermography (ULT). In this method, the thermographic system is coherently paired with a thermal source which is operated to result in a temperature modulation. This modulation is derived from a non-linear electrical signal generated by the lock-in module. LT is commonly employed in civil structures where the quantitative characterisation of the target is necessary. Several studies have developed NDT techniques to evaluate the efficiency of PT and LT, or their combination as tools for the defects characterisation. The key conclusion of all the previous studies that compared the two techniques was that PT was more effective spotting the larger defects, while LT enabled a more detailed picture of the defect. Also, PT and ULT were complimentarily employed to detect and characterize near surface cracking (Kordatos et al. 2013). The subsurface cracks were located by the IR camera, while the ultrasonic sensors obtained a more detailed assessment of the crack depth. Figure 2 represents the procedure of thermography technique.

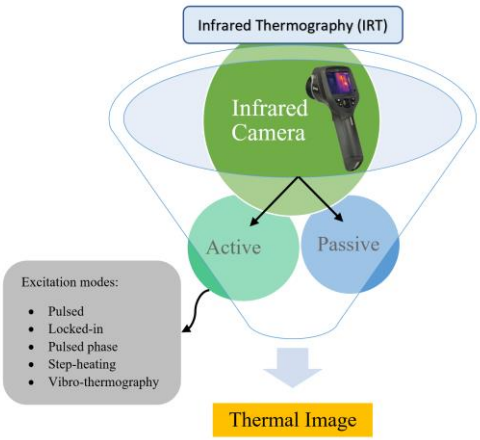

Figure 2: Schematic representation of passive and active thermography techniques

2.2 Basic concepts of electrical resistivity NDT

Electrical resistivity (ρ) of a material is defined as its ability to resist against transfer of ions when subjected to an electrical field. It is mostly dependent on the properties of concrete microstructure, such as pore size and shape of the interconnections (that is, tortuosity) (Layssi et al. 2015). Lower permeability causes by a finer pore network with less connectivity and ultimately leads to higher electrical resistivity. The range spanned by resistivity is one of the greatest of any material property (Hornbostel, Larsen, and Geiker 2013). For concrete, it differs from $10^6\ \Omega\ m$ for oven dried samples to $10\ \Omega\ m$ for saturated ones (Whitting and Nagi 2003). Electrical resistivity is the ratio between applied voltage (V) and resulting current (I) multiplied by a cell constant and the electrical current is carried by ions dissolved in the pore liquid (RILEM TC 154-EMC 2003; Polder 2001). Thus, it is a geometry independent property and an inherent characteristic of a material, as described in equation (1) (Layssi et al. 2015; RILEM TC 154-EMC 2003):

$$\rho = k.R = k.\left(\frac{V}{I}\right) \quad (1)$$

where R is the resistance of concrete; and k is a geometrical factor which depends on the size and shape of the sample as well as the distance between the probes on the testing device (Layssi et al. 2015). Two most important factors significantly affecting the concrete resistivity are the degree of saturation of the pore structure and temperature. Therefore, more pore water as well as more and wider pores results in lower concrete resistivity and higher temperature decreases the resistivity values (Polder 2001). Furthermore, adding reactive supplementary cementitious materials such as blast furnace slag, fly ash lead to lower

permeability and higher electrical resistivity due to reduction in capillary porosity and hydroxyl ions (OH^-). Both carbonation and chloride penetration also individually cause an increase in concrete resistivity in particular in Portland cement concrete but penetrated chloride impact is relatively small (Polder 2001).

2.2.1 ER Measurement techniques

Electrical resistivity measurements can be performed in several ways non-destructively: using electrodes positioned on a specimen surface, or placing an electrode-disc or linear array or a four probe square array on the concrete's surface. Types of device techniques that can be used typically to measure resistivity physically include (1) bulk electrical resistivity test (2) surface disc test (3) four-probe square array test (4) Wenner four-point line array test. In the bulk resistivity method (or uniaxial method), two electrodes are placed on the concrete surface (usually two parallel metal plates) with moist sponge in between (Figure 3.a). Generally, only standard cylinders/prismatic specimens or cores taken from existing structures are used in this method. The geometrical factor in this method can be obtained by following equation (2):

$$k = \frac{A}{L} \qquad (2)$$

where A is the cross-sectional area perpendicular to the current and L is the height of sample. Although, this non-destructive test takes only few seconds, its application is limited for field evaluation because electrodes access to opposite sides of the concrete element is not possible all the time. Other test methods that measure conductivity may use probes placed on the one side surface of the specimen.

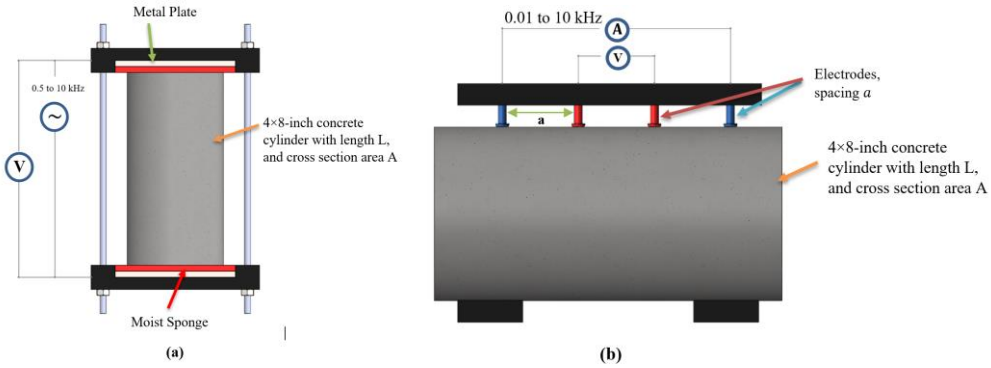

Figure 3: Electrical resistivity techniques: (a) two-point uniaxial method; and (b) four-point method

The Wenner probe technique was first introduced for the geologist's field in order to determine soil strata by Frank Wenner at the National Bureau of Standards in the 1910s and then modified through time for concrete application (Wenner 1916). In this technique, four equally spaced linear electrodes are used to measure the surface electrical resistivity of concrete (Figure 3.b). The two exterior electrodes apply an AC current to the concrete surface while the electrical potential is measured from the interior probes. The constant cell is defined as equation (3) for semi-infinite homogenous material (Layssi et al. 2015):

$$k = \gamma . a \qquad (3)$$

where a is the distance between the equally spaced electrodes and γ is the dimensionless geometry factor which is equal to 2π for semi-infinite concrete elements such as concrete slabs (Layssi et al. 2015). However, the geometry factor is different for tests conducted in a laboratory condition on small cylinders or cubic specimens. To measure the surface electrical resistivity, AASTHO TP 95-11 is the only specified standard which requires an electrode spacing of 1.5 inch (or 38 mm) with an AC frequency of 13 Hz (AASHTO TP 95 2011).

3 EXPERIMENTAL PROGRAM

This study investigated the temperature response and electrical resistivity for steel reinforced concrete slabs with implanted defects at varying depths. Four RC slabs were constructed with two different thicknesses (100 and 150 mm thick) in Civil Engineering Material Facility (CEMF) at UVic. The specimens' length and width are 1800 and 460 mm while the maximum aggerate size is 12.5 mm. The w/c ratio used was 0.42 in all types of concrete and the mix design, which represents a typical mix used in the field with target strength of about 32 MPa, is given in Table 1.

Table 1: Mix proportions of reinforced concrete slabs

Composition	Cement	Fly Ash	Gravel	Sand	Water	w/c
Quantity (Kg/m^3)	276	69	1055	815	140	0.42

A mesh of 10 mm bars at 130 mm spacing and 12.5 mm depth from bottom surface was used as reinforcement for slabs. Artificial defects and cracks were created and implanted inside the two specimens before casting while two other samples used as control. Figure 4 shows the locations and depth of defects inside the slab. The defects are modeled as foam bars (white) and delocalised aggregates (teal).

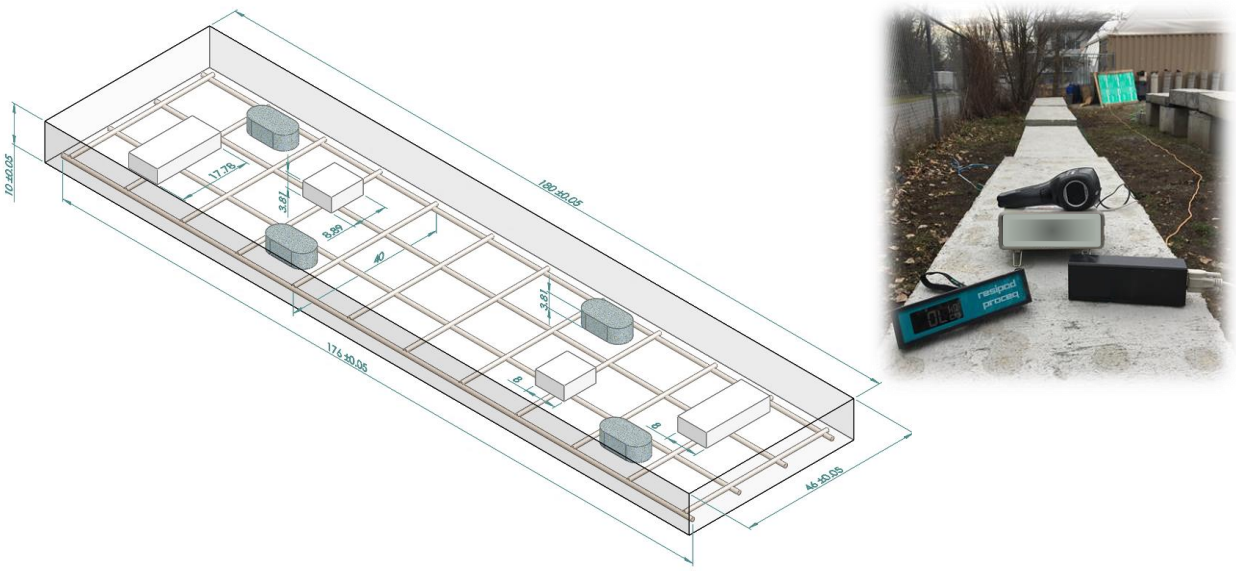

Figure 4: 3D model of artificial defects in steel reinforced concrete slab

In the experimental setup, FLIR i7 infrared camera with a spectral range of 7.5 -13 µm, imaging frequency of 9 Hz, spatial resolution of 3.71 mrad and a thermal sensitivity of <0.1℃ has been used for taking thermal images from surface of reinforced concrete slabs. Thermal induction of the slabs was applied using temperature controlled heat blankets. The blankets were wrapped around the selected slabs for 16 hours at 40℃ columns to simulate active thermography. Each slab was unwrapped before testing and were cooled at air temperature for 4 hours.

In this study, surface electrical resistance (R, in Ω) measurements were performed on slab's surface by commercially available 4 point Wenner probe resistivity meter, manufactured by Proceq, following procedure detailed in AASHTO TP95-11 (AASHTO TP 95 2011). Then, the values of resistivity (ρ) can be calculated as: $\rho = k.R$, where k is a geometrical factor that depends on the shape of the sample. Five resistivity readings have been taken from the same positons and each time, four electrodes were moved at

least a few millimeters between readings. All slabs were saturated before testing to ensure active electrical conduction according to AASHTO TP95-11.

4 RESULTS AND DISCUSSION

4.1 General

The following results outline IR and ER measurements to investigate defect evaluation. Each IR and ER measurements have been taken 5 cm away from the slab sides to mitigate any edge effects. ER testing was conducted on a total of number of 210 points spaced 5 cm apart. All IR images are divided into 6 equal images taken along the slab to create a collaged of the slabs top surface. Table 2 shows the IR image properties before testing.

Table 2: Thermal image properties during testing

Image Properties	Emissivity	Ambient Temperature	Reflected Temperature	Humidity
	0.972	8.4 °C	20 °C	80%

The average temperature for heated control and defect slabs after unwrapping is 29℃. The ambient temperature was 8.4℃. Figure 5 shows the thermal IR image after unwrapping. Figure 5 (a) indicates a temperature difference between the selected heated slabs for testing (18℃) and other unheated reference slabs (8℃). The capturing distance of the image, however, does not reflect on the true emitted temperature from the slab. Figure 5 (b) shows the average temperature of slabs inspected at height of 1m from the top surface of the slab. The average temperature for heated control and defect slabs before testing is 14℃.

A difference in the overall heated volume of concrete can be recognised for 15 cm slabs as shown in Figure 5(c). The IR image shows a temperature gradient between 9 – 20℃ from each side moving towards the center of the slab respectively. This can be attributed to side cooling since the thermal blanket was unable to cover the heating element along the side of the slab. Moreover, this can be interpreted through the high rate. dissipated heat from a larger volume when compared to 10 cm slabs. Results throughout this study showed that the theromgraphic IR images indicate the presence of foam bar defects however, IR did not capture the delocalised aggerates yet, ER appeared to capture the relative change in resistivity on the surface.

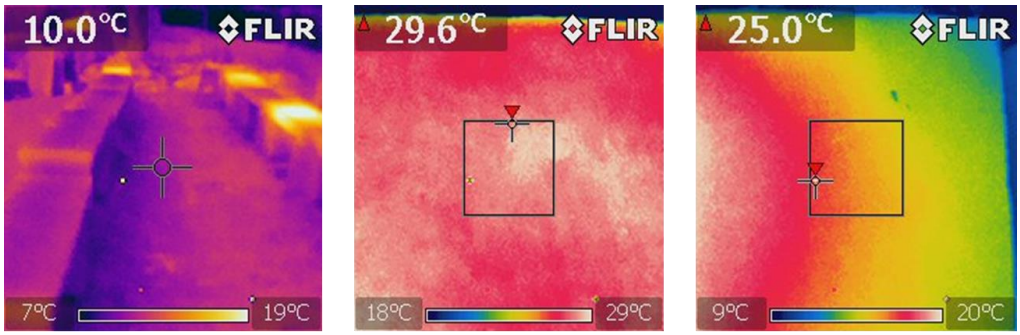

(a) (b) (c)

Figure 5: a) IR image of heated and reference slabs b) Average slab temperature before cooling c) Side cooling of 150 mm slabs

4.2 Non-destructive Evaluation of Slabs

4.2.1 Electrical Resistivity

Through the ER analysis shown in Figure 8, higher resistivity values (150-200 kΩ.cm) can be ascribed to irregularity along the surface of the slab. The foam defects shown at the 50 cm and 130 cm span length respectively have an extra thickness of approximately 5 mm on the concrete surface. This can be a result of the foam bar moving during casting, as shown through the IR analysis, thus deforming the surface. At the 160cm span, the ER values indicate lower resistivity since the surface at this edge affected by moisture.

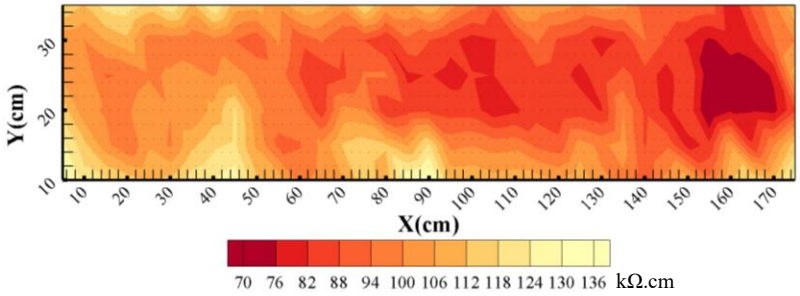

Figure 6: Resistivity map for 10 cm slab thickness (Control)

The average resistivity and standard deviation is shown in Table 3. Both the control and defect 100 mm thick slabs show a close average resistivity however, the standard deviation of the defect slabs was twice that of the control. The resistivity map for the defect 100 mm slab is shown in the next section for a comparison between IR and ER.

Table 3: Average surface electrical resistivity for control and defect slabs

Slab	Surface Electrical Resistivity (kΩ.cm)			
	Maximum	Minimum	Mean	St. Dev
C100	137.2	68.5	98.331	13.711
D100	196.6	50.0	101.735	26.501

4.2.2 Infrared Thermography

Internal Defect Identification

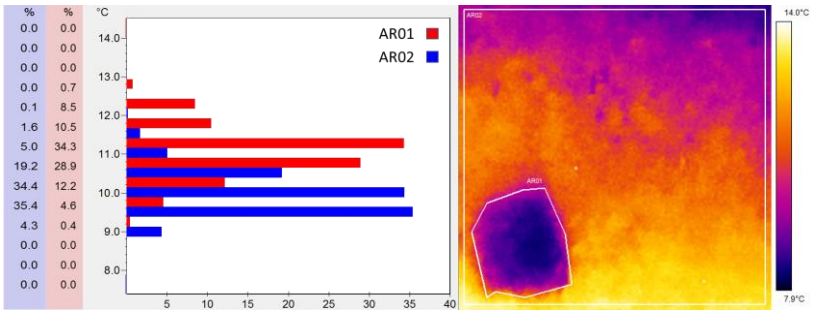

Area	Max – Min [°C]	Avg. [°C]	St.Dev [°C]
AR01	17.9 – 9.2	10.9	0.6
AR02	11.6 – 9.2	10.1	0.5

Figure 7: Box analysis histogram of defect in relation total surface area

Figure 7 demonstrates a surface box plot analysis of the defect area with respect to 130×130 pixels and includes the maximum, minimum, average temperature, and standard deviation of each area. The blue bars in the above histogram show the frequency of the defect temperature in comparison with the 130 ×130-pixel image average. From the average temperature of 10.9°C for the box analysis, the defect average temperature shows a noticeable percentage of 28.9% from the total area.

In Figure 8, the IR imaging clearly indicates the foam bar presence throughout the defect beams. Moreover, the thermographic image outlines that the foam defects possibly have moved during casting by changing their orientation. In addition, ER readings present higher or lower values in the defected zone. However, depending on the moisture content of implanted anomalies, the side facing sun loses more moisture, and thus showing higher resistivity values. Dashed lines also specify the location of artificial defects which in both IR and ER contour maps pass through the same spot. In general, the variations in resistivity results were observed to be higher in the defected slab compare to control one. Consequently, these two NDT methods show a strong correlation in detecting irregularities/defects and can be a good indicator for locating defects/voids.

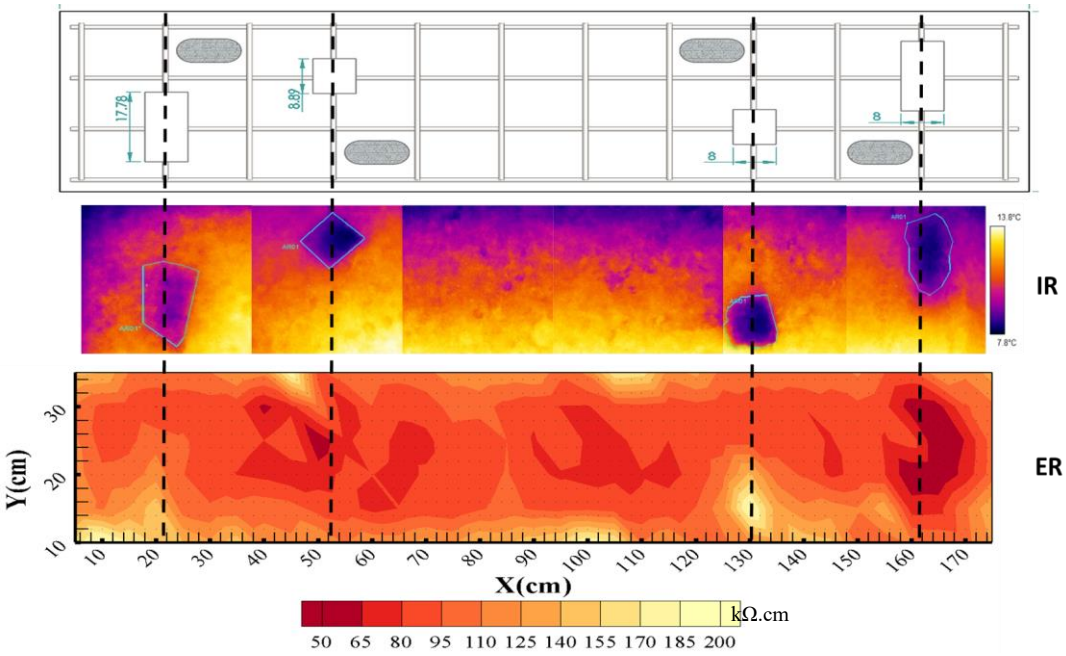

Figure 8: Identification of defect using both IR and ER NDT methods

Surface Defect Identification

Through IR imaging, surface pore defects can be distinguished. **Error! Reference source not found.** shows the image of the 10 cm slab with localized pore defects along the surface. A box and spot analysis allowed simple identification of the pore locations. The surface pores range between 7.9 – 9.4℃ with spot identification while the total surface temperature range is between 7.7 – 18.5℃. This is inline with the detection of voids and surface irregularities by (Maierhofer, Arndt, and Röllig 2007).

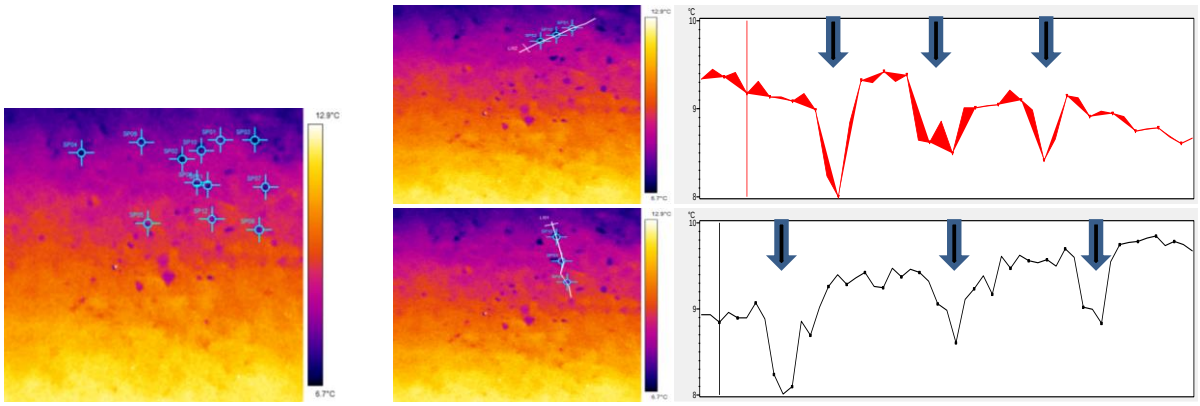

Figure 9: Pore allocation and line analysis showing pore distribution with temperature

Defect analysis of 15 cm thick slabs

Figure *10* shows the IR testing carried out on the15 cm thick concrete slabs of the same control and defect pattern. The IR and ER analyses show no clear indication of any defects along the slab. Since the IR camera was unable to detect the temperature variation between the applied defects and concrete, the ER testing was discontinued for the 150 mm concrete slabs.

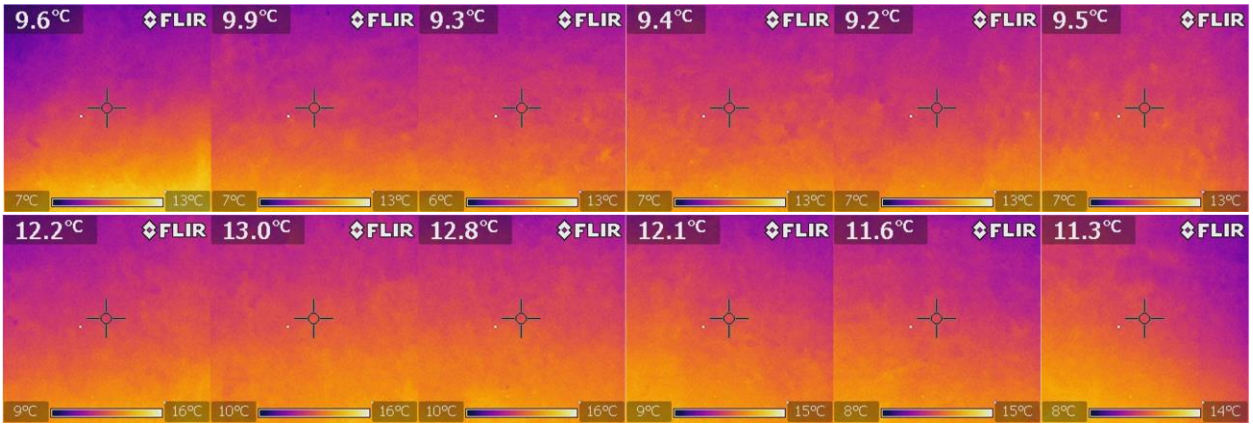

Figure 10: Temperature gradient of control (top) and defect (bottom) 15 cm reinforced concrete slabs

5 CONCLUSION

ER and IR can be used as means of identification of both surface anomalies and internal defects respectively. Irregular surface structure and porosity can be indicated through surface resistivity values. IR can be substantially used to identify surface pores and internal defects at 10 cm thick field slab. Image analysis of pore surfaces indicated an obvious difference between the pores and internal temperature. This presented that active pulse thermography can be employed efficiently for thermal induction of reinforced concrete structures. Both non-destructive methods however were inconclusive for detecting internal defects as the thickness of the slabs increase to 15 cm.

6 REFERENCES

AASHTO TP 95. 2011. “Method of Test for Surface Resistivity Indication of Concrete’s Ability to Resist Chloride Ion Penetration.” *American Association of State Highway and Transportation Officials*.

ASTM D4788-03. 2013. “Standard Test Method for Detecting Delaminations in Bridge Decks Using Infrared Thermography.” ASTM International.

Azarsa, Pejman, and Rishi Gupta. 2017. “Electrical Resistivity of Concrete for Durability Evaluation – Review.” *Advances in Materials Science and Engineering*.

Balaras, C.A., and A.A. Argiriou. 2002. “Infrared Thermography for Building Diagnostics.” *Energy and Buildings* 34 (2): 171–83. doi:10.1016/S0378-7788(01)00105-0.

Brown, Jeff R., and H.R. Hamilton. 2013. “Quantitative Infrared Thermography Inspection for FRP Applied to Concrete Using Single Pixel Analysis.” *Construction and Building Materials* 38 (January): 1292–1302. doi:10.1016/j.conbuildmat.2009.12.016.

Büyüköztürk, Oral. 1998. “Imaging of Concrete Structures.” *NDT & E International* 31 (4): 233–43. doi:10.1016/S0963-8695(98)00012-7.

Carosena Meola and Giovanni M Carlomagno. 2004. “Recent Advances in the Use of Infrared Thermography.” *Measurement Science and Technology* 15 (9): R27.

Cheng, Chia-Chi, Tao-Ming Cheng, and Chih-Hung Chiang. 2008. “Defect Detection of Concrete Structures Using Both Infrared Thermography and Elastic Waves.” *Automation in Construction* 18 (1): 87–92. doi:10.1016/j.autcon.2008.05.004.

Hornbostel, Karla, Claus K. Larsen, and Mette R. Geiker. 2013. “Relationship between Concrete Resistivity and Corrosion Rate – A Literature Review.” *Cement and Concrete Composites* 39 (May): 60–72. doi:10.1016/j.cemconcomp.2013.03.019.

Kordatos, E. Z., D. V. Soulioti, M. Strantza, T. E. Matikas, and D. G. Aggelis. 2013. “Thermography and Ultrasound for Characterizing Subsurface Defects in Concrete.” In *Nondestructive Testing of Materials and Structures*, edited by Oral Büyüköztürk, Mehmet Ali Taşdemir, Oğuz Güneş, and Yılmaz Akkaya, 193–98. Dordrecht: Springer Netherlands. http://dx.doi.org/10.1007/978-94-007-0723-8_28.

Kylili, Angeliki, Paris A. Fokaides, Petros Christou, and Soteris A. Kalogirou. 2014. “Infrared Thermography (IRT) Applications for Building Diagnostics: A Review.” *Applied Energy* 134 (December): 531–49. doi:10.1016/j.apenergy.2014.08.005.

Layssi, Hamed, Pouria Ghods, Aali R. Alizadeh, and Mostafa Salehi. 2015. “Electrical Resistivity of Concrete.” *Concrete International*, May.

Maierhofer, Ch., R. Arndt, and M. Röllig. 2007. “Influence of Concrete Properties on the Detection of Voids with Impulse-Thermography.” *Infrared Physics & Technology* 49 (3): 213–17. doi:10.1016/j.infrared.2006.06.007.

Maldague, Xavier. 2001. “Theory and Practice of Infrared Technology for Nondestructive Testing.”

Meola, Carosena, and Giovanni Maria Carlomagno. 2006. “Application of Infrared Thermography to Adhesion Science.” *Journal of Adhesion Science and Technology* 20 (7): 589–632. doi:10.1163/156856106777412491.

Poblete, A., and M. Acebes Pascual. 2007. “Thermographic Measurement of the Effect of Humidity in Mortar Porosity.” *Infrared Physics & Technology* 49 (3): 224–27. doi:10.1016/j.infrared.2006.06.009.

Polder, Rob B. 2001. “Test Methods for on Site Measurement of Resistivity of Concrete — a RILEM TC-154 Technical Recommendation.” *Construction and Building Materials* 15 (2–3): 125–31. doi:10.1016/S0950-0618(00)00061-1.

Rajabipour, Farshad, Jason Weiss, and Dulcy M. Abraham. 2004. “Insitu Electrical Conductivity Measurements to Assess Moisture and Ionic Transport in Concrete (A Discussion of Critical Features That Influence the Measurements).” In . RILEM Publications SARL. doi:10.1617/2912143926.049.

Ranade, Ravi, Jie Zhang, Jerome P. Lynch, and Victor C. Li. 2014. “Influence of Micro-Cracking on the Composite Resistivity of Engineered Cementitious Composites.” *Cement and Concrete Research* 58 (April): 1–12. doi:10.1016/j.cemconres.2014.01.002.

RILEM TC 154-EMC. 2003. “Recommendations of RILEM TC 154-EMC: Electrochemical Techniques for Measuring Metallic Corrosion Half-Cell Potential Measurements - Potential Mapping on Reinforced Concrete Structures.” *Materials and Structures* 36 (261): 461–71. doi:10.1617/13718.

Sengul, Ozkan. 2014. “Use of Electrical Resistivity as an Indicator for Durability.” *Construction and Building Materials* 73 (December): 434–41. doi:10.1016/j.conbuildmat.2014.09.077.

Sun, J. G. 2006. “Analysis of Pulsed Thermography Methods for Defect Depth Prediction.” *Journal of Heat Transfer* 128 (4): 329. doi:10.1115/1.2165211.

Titman, D.J. 2001. “Applications of Thermography in Non-Destructive Testing of Structures.” *NDT & E International* 34 (2): 149–54. doi:10.1016/S0963-8695(00)00039-6.

Washer, GA. 1998. “Developments for the Non-Destructive Evaluation of Highway Bridges in the USA.” *NDT&E Int* 31 (4): 245–49.

Wenner, F. 1916. “A Method of Measuring Earth Resistivity.” *Bulletin of the Bureau of Standards* 12 (4): 469. doi:10.6028/bulletin.282.

Whitting, D. A., and M. A. Nagi. 2003. “Electrical Resistivity of Concrete.” 2457. Sookie, IL: Portland Cement Association.